

Binding Mode of TMC-95A Analogues to Eukaryotic 20S Proteasome

Markus Kaiser,^[a] Michael Groll,^[b] Carlo Siciliano,^[a] Irmgard Assfalg-Machleidt,^[b] Elisabeth Weyher,^[a] Jun Kohno,^[c] Alexander G. Milbradt,^[a] Christian Renner,^[a] Robert Huber,^[a] and Luis Moroder*^[a]

The complex thermodynamics that govern noncovalent protein–ligand interactions are still not fully understood, despite the exponential increase in experimental structural data available from X-ray crystallography and NMR spectroscopy. The eukaryotic 20S proteasome offers an ideal system for such studies as it contains in duplicate three proteolytically active sites with different substrate specificities. The natural product TMC-95A inhibits these proteolytic centers noncovalently with distinct affinities. X-ray crystallographic analysis of the complexes of the yeast proteasome core particle with this natural inhibitor and two synthetic analogues clearly revealed highly homologous hydrogen-bonding networks involving mainly the peptide backbone despite the strongly differentiated binding affinities to the three active sites of the 20S proteasome. The natural product and the two ana-

logues are constrained in a rigid β -type extended conformation by the endocyclic biaryl clamp, which preorganizes the peptide backbone for optimal adaptation of the ligands to the active site clefts and thus favors the binding processes entropically. However, the biaryl clamp also dictates the orientation of the P1 and P3 residues and their mode of interaction with the protein binding subsites. This limitation is optimally solved in TMC-95A with the conformationally restricted (Z)-prop-1-enyl group acting as P1 residue, at least for the chymotrypsin-like active site; however, it critically affects the inhibitory potencies of the analogues, thus suggesting the use of less-rigid endocyclic clamps in the design of proteasome inhibitors that allow for a better presentation of residues interacting with the active site clefts of the enzyme.

Introduction

The primary component of the intracellular protein degradation pathway is the proteasome, which acts as an effective machinery for regulating vital cell processes such as cell-cycle progression, apoptosis, and NF- κ B activation.^[1] The proteasome is a multicatalytic protease complex containing various active sites within its central core (CP, core particle; 20S proteasome) and a 19S regulatory complex which is attached to the CP and is responsible for substrate recognition and unfolding. Structure assembly and enzymatic mechanisms have been elucidated only for the CP, whereas the organization of the regulatory particle is less well understood.^[2] The CP is a large barrel-shaped protein complex consisting of four rings of subunits which are tightly packed in an $\alpha_{1-7}\beta_{1-7}\beta_{1-7}\alpha_{1-7}$ arrangement. While the α subunits exert substrate gating functions,^[3] the β subunits act as the proteolytic centers, and only the fully assembled CP is able to degrade the unfolded proteins into small-sized peptides in a processive manner.^[4] In eukaryotic CPs, three β -type subunits (β_1 , β_2 , and β_5) are autolytically processed to generate the enzyme active sites, whereas the other four β -type subunits remain inactive. Within the CP, each pair of proteolytically active subunits shows a certain degree of substrate specificity with the β_1 subunits particularly responsible for post-glutamyl peptide hydrolyzing (PGPH) caspase-like activity, the β_2 subunits exhibiting trypsin-like activity, and the β_5 subunits chymotrypsin-like activity.^[5] The S1 pockets of these subunits are the major specificity determinants and are appropriately polar and sized to accommodate acidic,

basic, and apolar P1 side chains, respectively, but also bind noncomplementary residues in a manner consistent with the low specificity of the proteasome.^[2,5b] This last property raises the main difficulties in the design of highly selective inhibitors even though the surface characteristics of the substrate binding subsites are known from X-ray crystallographic studies and the binding modes of various small-sized synthetic and natural inhibitors have been elucidated.^[2,6]


Because of the promising therapeutic potential of proteasome inhibition,^[1b,c,7] much attention has been paid to the development of synthetic inhibitors and to the discovery of natural ligands. Besides the synthetic inhibitors derived from 2-aminobenzylstatine,^[8] only the secondary metabolites TMC-95A

[a] Dr. M. Kaiser,^{*} Dr. C. Siciliano, E. Weyher, Dipl.-Biochem. A. G. Milbradt, Dr. C. Renner, Prof. R. Huber, Prof. L. Moroder
Max-Planck-Institut für Biochemie
Am Klopferspitz 18, 82152 Martinsried (Germany)
Fax: (+49) 89-8578-2847
E-mail: moroder@biochem.mpg.de

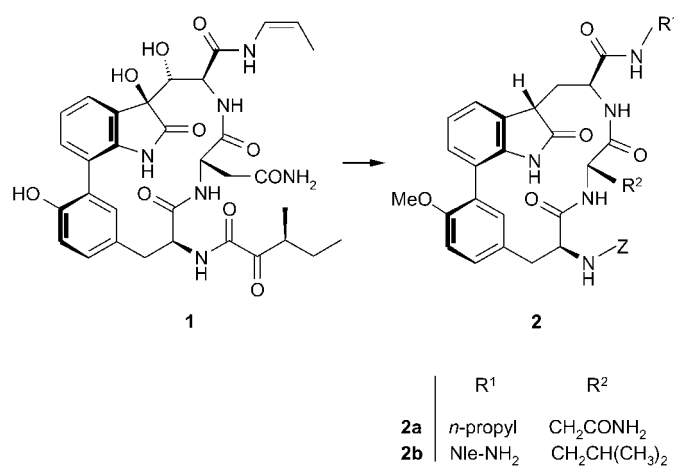
[b] Dr. M. Groll,^{*} Dr. I. Assfalg-Machleidt
Adolf-Butenandt-Institut der Ludwig-Maximilians-Universität
80336 München (Germany)

[c] Dr. J. Kohno
Discovery Research Laboratory, Tanabe Seiyaku Co. Ltd.
2-2-50 Kawagishi, Toda-shi, Saitama 335-8505 (Japan)

[*] Both authors contributed equally to this work.

 Supporting information for this article is available on the WWW under <http://www.chembiochem.com> or from the author.

and its diastereoisomers TMC-95B/C/D from *Apiospora montagnei* have been recognized as potent reversible inhibitors of human 20S proteasome.^[9] TMC-95A (**1**) is a cyclic tripeptide derivative which is constrained into a 17-membered-ring structure by an endocyclic biaryl system derived from tyrosine and a highly oxidized tryptophan side chain (Scheme 1). Its nonco-



Scheme 1. Structure of the natural product TMC-95A (**1**) and of the related synthetic analogues **2a** and **2b**; according to the X-ray structure of the TMC-95A–yeast CP complex the R₁ and R₂ residues should act as P1 and P3 residues, respectively, and thus interact with the S1 and S3 subsites of the proteasome active sites; Z = benzyloxycarbonyl.

valent binding to the β 1, β 2, and β 5 active sites of yeast CP has been characterized by X-ray crystallographic analysis.^[6a] The interactions of the inhibitor with the active site clefts consist mainly of hydrogen bonds between its rigid extended peptide backbone and the protein to form an antiparallel β -sheet structure with an additional hydrogen bond involving the oxindole group. The tyrosine residue of the inhibitor interacts only weakly with the shallow hydrophobic S4 subsites of all active sites, while the hydroxy group is exposed to the solvent. Similarly, the N-terminal 3-methyl-2-oxopentanoyl group is exposed to the bulk solvent without apparent interactions with the protein. Thus, the conformationally restricted C-terminal (*Z*)-prop-1-enyl moiety (P1 residue) and the central asparagine (P3 residue) should be mainly responsible for the significantly differentiated binding affinities of TMC-95A to the three active sites.^[6a] A minimal TMC-95 core structure (Scheme 1, **2**) was therefore derived from these crystallographic data and from a comparison with the binding mode of epoxomicin.^[6a,b]

This synthetically less challenging scaffold was expected to represent a promising lead for the development of a new class of noncovalently binding proteasome inhibitors. In the present study, a first set of related derivatives were synthesized and analyzed for their inhibitory potencies and mode of binding to yeast 20S proteasome. The information derived from the X-ray data suggests less rigid scaffolds are more suitable for an optimal display of groups interacting with the binding subsites of the β 1, β 2, or β 3 active centers.

Results

Design and synthesis of TMC-95A analogues

The X-ray-derived minimal core structure of TMC-95A (**2**, Scheme 1) lacks the 3-methyl-2-oxopentanoyl group at the N-terminus, the synthetically challenging *cis*-enamide group at the C-terminus, and the two hydroxy groups of the tryptophan moiety; however, the oxindole group is retained since it is hydrogen bonded to the protein surface. Similarly, the tripeptide backbone is retained because of its essential contribution to the hydrogen-bonding networks at the three active sites of the 20S proteasome. To analyze the roles of the P1 and P3 residues in modulating the inhibitor specificities for the trypsin-, chymotrypsin-, and caspase-like activities, this scaffold was substituted C-terminally with an *n*-propyl group (acting as the P1 residue) and N-terminally with a benzyloxycarbonyl (Z) N-protecting group, while the central Asn residue of TMC-95A was kept as the P3 residue (**2a**) (for a preliminary communication see ref. [10]). In a second analogue (**2b**), the (*Z*)-prop-1-enyl group of TMC-95A was replaced by a norleucine (Nle) side chain and Asn by Leu with the aim of increasing the specificity for the chymotrypsin-like active site. In the case of calpain inhibitor I (Ac-Leu-Leu-Nle-H)^[11] and peptide vinylsulfones,^[12] similar P1 and P3 residues were found to be well suited for this purpose. The superimposition of the X-ray structures of the latter inhibitors^[2b,6c] with that of TMC-95A^[6a] in complexes with yeast CP showed an almost identical peptide backbone display, thus suggesting similar orientations of the Leu and Nle side chains when incorporated into TMC-95A to act as P1 and P3 residues, respectively. To facilitate the synthesis of these analogues, the tyrosine hydroxy group was methylated.

Model studies showed that the synthesis of the biaryl system proceeded with better yields by a Suzuki coupling between a phenol boronic acid and a halogenated indole rather than vice versa.^[13] Therefore, the required intermediate, 7-bromo-L-tryptophan, was synthesized by enzymatic procedures from 7-bromoindole and L-serine with tryptophan synthase^[14] by following essentially the method reported for the enzymatic synthesis of chloro-L-tryptophans.^[15] Because of the low yields and the need for recombinant tryptophan synthase, a new chemical synthesis was developed for the 7-bromo-L-tryptophan derivative, which is based on a previously reported synthesis of β -(1-azulenyl)-L-alanine^[16] (see Supporting Information). Macrolactamizations of linear precursors containing the biaryl system of TMC-95A (with its highly oxidized Trp component) were reported to proceed in good yields.^[17] Therefore, the two analogues **2a** and **2b** were prepared by following the synthetic route reported in our preliminary communication.^[10] Briefly, this involves cyclization of the biaryl-containing precursors upon oxidation of the indole group to the oxindole; this allows sp³ hybridization of the indole C3 atom as required for ring closure to the constrained 17-membered macrocycle. In fact, molecular dynamics (MD) simulations with the (*R*)-C3 diastereoisomer confirmed that for steric reasons cyclization is only possible with the (*S*)-C3 diastereoisomer.

Highly convergent solution structures were calculated for the analogues **2a** and **2b** with NMR-derived distance constraints (Figure 1). The root mean square deviation (rmsd) values of 0.065 Å and 0.055 Å for backbone atoms and 0.19 Å and 0.15 Å for the heavy atoms of the aromatic residues of **2a** and **2b**, respectively, reflect the rigidity of the cyclic structure. A comparison of these structures with that of TMC-95A in the yeast CP-bound state^[6a] reveals differences only in the spatial display of the P1 and P3 residues (Figure 1). Thus, from a structural point of view, these analogues were expected to bind to the 20S proteasome in a mode very similar to TMC-95A and with a minimum of entropic penalty.

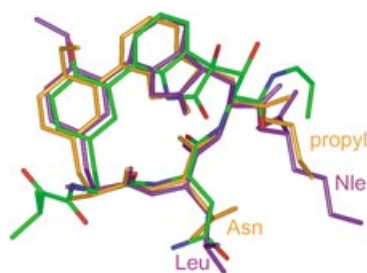


Figure 1. Comparison of NMR-derived structures of the TMC analogues **2a** (orange) and **2b** (violet) with the structure of TMC-95A (green/normal atom colors) in the crystallized complex.^[6a] Backbone atoms were used for the superimposition. The rmsds (referenced to the natural product) of 0.44 Å and 0.53 Å were calculated for **2a** and **2b**, respectively. The N-terminal benzoyloxycarbonyl group is omitted in both analogues.

Inhibition of human, bovine, and yeast 20S proteasome by TMC-95A

In the case of proteasome CPs, kinetic parameters are known to depend significantly on the assay conditions and enzyme preparation. For the present study, the yeast CP was prepared in high homogeneity by a newly optimized procedure (see Experimental Section). Inhibition of the chymotrypsin-, trypsin-, and caspase-like activities of this yeast CP by TMC-95A, **2a**, **2b**, and calpain inhibitor I (Ac-Leu-Leu-Nle-H) was determined in the presence of detergents to allow comparison with kinetic parameters reported for TMC-95A^[9a] and its synthetic replica^[18] using human and bovine 20S proteasome, respectively. Under these conditions, TMC-95A was found to inhibit the chymotrypsin-like activity of yeast CP, human,^[9a] and bovine enzymes^[18] with practically identical potency (Table 1). However, the trypsin-like activity of yeast CP is inhibited by TMC-95A with significantly higher potency than that of the human and bovine species. The opposite is observed for caspase-like activity: the bovine and human enzymes are more potently inhibited by TMC-95A. In a similar manner, differences are observed when inhibiting yeast and human CPs with calpain inhibitor I (Table 1). These results suggest that both the potency and specificity of proteasome inhibitors depend significantly on the source of the enzyme despite the strong sequence homologies and the highly convergent 3D structures of 20S proteasomes from different species.^[2,19]

Table 1. Inhibition of yeast^[a] (K_i [μM]), bovine^[b] (K_i [μM]), and human 20S proteasome^[c] (IC_{50} [μM]) by TMC-95A and Ac-Leu-Leu-Nle-H.

Inhibitor	Chymotrypsin-like activity (β_5 subunit)	Trypsin-like activity (β_2 subunit)	Caspase-like activity (β_1 subunit)
TMC-95A (1)	$0.0011 \pm 0.00007^{[a]}$ $0.0011 \pm 0.0001^{[b]}$ $0.0054^{[c]}$	$0.043 \pm 0.007^{[a]}$ $0.81 \pm 0.12^{[b]}$ $0.20^{[c]}$	$0.65 \pm 0.023^{[a]}$ $0.029 \pm 0.004^{[b]}$ $0.06^{[c]}$
Ac-Leu-Leu-Nle-H	$0.630 \pm 0.025^{[a]}$ $6.6^{[c]}$	$230 \pm 27.8^{[a]}$ $6.0^{[c]}$	$\geq 1800^{[a]}$ $21^{[c]}$

[a] Values determined in the present study with the yeast CP prepared according to an optimized protocol. [b] Values reported from ref. [18]. [c] Values reported from ref. [9a].

Inhibition of yeast 20S proteasome by TMC-95A analogues

Replacement of the conformationally restricted (*Z*)-prop-1-enyl moiety of TMC-95A with the flexible *n*-propyl chain (acting as the P1 residue) leads to a 20-fold decrease of binding affinity for the β_5 subunits (chymotrypsin-like activity) of bovine 20S proteasome ($K_i = 24 \text{ nM}$).^[18] For the analogue **2a**, which contains the same C-terminal replacement, a 500-fold lower inhibition of yeast CP was observed relative to TMC-95A (Table 2).

Table 2. Inhibition of yeast 20S proteasome (K_i [μM]) by TMC-95A and its analogues **2a** and **2b**.

Inhibitor	Chymotrypsin-like activity (β_5 subunit)	Trypsin-like activity (β_2 subunit)	Caspase-like activity (β_1 subunit)
TMC-95A (1)	0.0011 ± 0.00007	0.043 ± 0.007	0.65 ± 0.023
2a	0.55 ± 0.029	0.15 ± 0.005	90 ± 8.4
2b	1.2 ± 0.06 (K_i^{\dagger}) 2.4 ± 0.09	5.3 ± 0.6 (K_i^{\dagger}) 22 ± 2.6	≥ 1000

Compared to TMC-95A, the compound **2a** contains, in addition to the flexible *n*-propyl chain, an N-terminal benzylurethane instead of the alkylketoamide group. Moreover, it lacks the two hydroxy groups at the tryptophan moiety. According to the X-ray structures (vide infra), neither the N-terminal replacement nor the absence of the two hydroxy groups can account per se for the additional factor of 25. A combination of both modifications therefore has to be responsible for the significantly lower affinity observed.

The inhibitory potencies of TMC-95A for the trypsin- and caspase-like activities of bovine 20S proteasome (Table 1) are again lowered by one order of magnitude upon replacing the (*Z*)-prop-1-enyl with the *n*-propyl chain.^[18] In the case of yeast CP, inhibition of the trypsin-like activity by **2a** is reduced only by a factor of 3–4 compared to TMC-95A (Table 2), but inhibition of the caspase-like activity is reduced by two orders of magnitude. These results confirm the existence of structural differences between the β_1 active sites of proteasomes from different species.

Replacement of the (Z)-prop-1-enyl group with Nle-amide (acting as the P1 residue) and of Asn with Leu (acting as the P3 residue) to specifically address the $\beta 5$ subunits proved to be an unfavorable approach. Inhibition of both the chymotrypsin- and trypsin-like activities by **2b** shows two phases with temporary K_i values of $1.2 \mu\text{M}$ and $5.3 \mu\text{M}$, which then convert to the higher values of $2.4 \mu\text{M}$ and $22 \mu\text{M}$, respectively. This observation can only be explained by a chemical transformation of **2b** derived from hydrolysis of the C-terminal amide if this scissile amide bond is positioned in substrate-like mode upon binding of **2b** to the active sites. Mass spectrometry studies confirmed the occurrence of this hydrolysis. By monitoring the amide hydrolysis with HPLC upon exposure of **2b** to yeast proteasome in the presence of substrate, a $t_{1/2}$ value of 27 min was derived (see Experimental Section). The resulting carboxylate apparently leads to a less favorable binding of the inhibitor to $\beta 5$ and in an even more pronounced manner to the $\beta 2$ subunit. The latter observation is rather surprising, since in crystals of the CP-inhibitor complexes, compound **2b** binds to the $\beta 2$ subunit in a mode similar to **2a** and TMC-95A, but to the $\beta 5$ subunits in a different manner (vide infra).

The binding affinity of **2b** for $\beta 1$ subunits is even more reduced than in the case of $\beta 2$ and $\beta 5$. This may well be explained by the presence of an Arg residue in the S1 pocket of the $\beta 1$ subunits, which dictates selectivity for negatively charged residues and thus induces the caspase-like activity.

X-ray crystallographic analysis of proteasome complexes with **2a** and **2b**

Well-defined electron density maps were obtained from crystals of the yeast CP complexed with the inhibitors **2a** and **2b**, as illustrated in Figure 2 for the $\beta 5$ active site complexed by **2b**. The electron density maps clearly revealed the presence of the inhibitor **2a** in the $\beta 1$, $\beta 2$, and $\beta 5$ active sites (Figure 3), whereas **2b** was not detectable in the $\beta 1$ active site despite the high inhibitor concentrations (5 mM) used in the soaking experiments. This fact further confirms the weak binding of **2b**

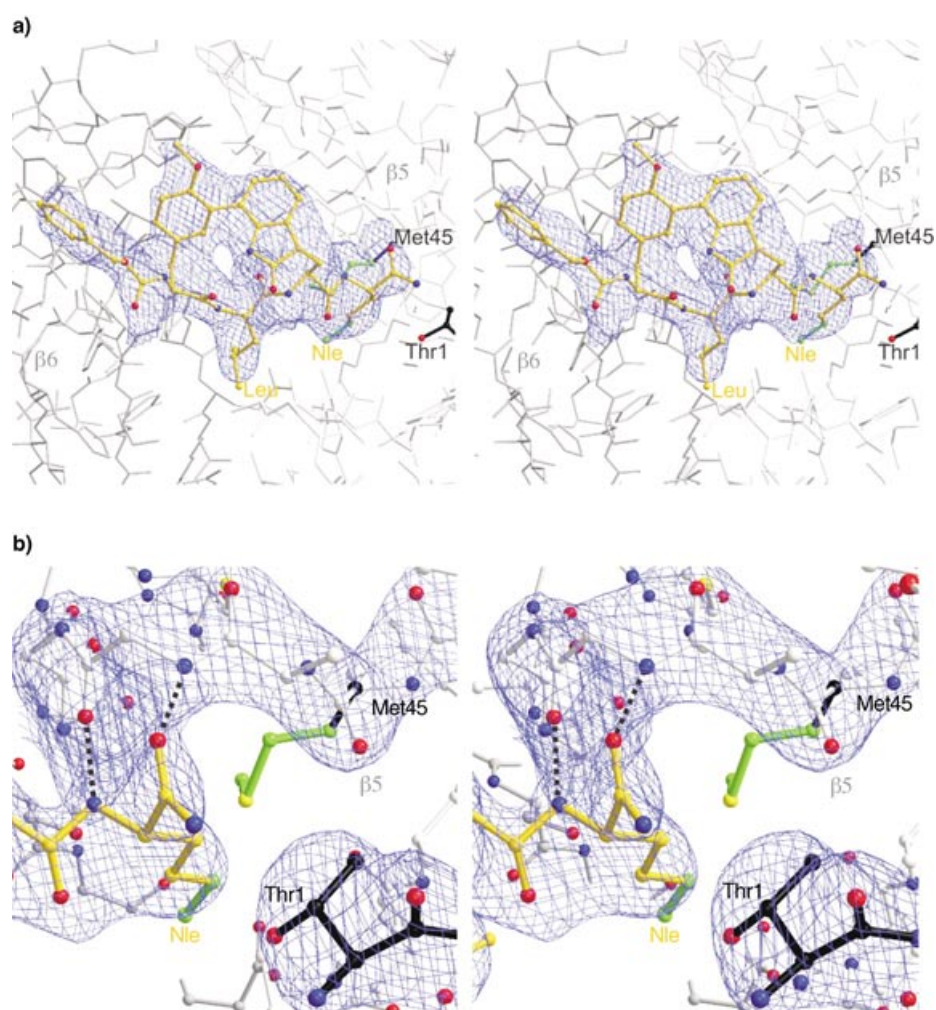


Figure 2. a) Noncovalent binding of **2b** to subunit $\beta 5$ of the yeast 20S proteasome. **2b** is depicted in yellow and shown in stereo mode, together with its unbiased electron density. The active site threonine is highlighted in black. Met45, which is in particular responsible for the specificity of the S1 pocket, is shown in black, whereas the disordered side chain of this residue is colored in green. b) Close up view of the S1 pocket of subunit $\beta 5$ in complex with **2b**. The bulky Nle side chain of the inhibitor induces the flexibility of the side chain of Met45 in subunit $\beta 5$.

to the caspase-like active site. After refinement, resolutions of 3.1 \AA and 2.6 \AA were obtained for the CP complexes with **2a** and **2b**, respectively (for refinement statistics see Table 3). To facilitate a comparison of the binding modes of TMC-95A, **2a**, and **2b** to yeast CP at the various active sites, hydrogen-bonding pairs are listed in Table 4.

Binding of inhibitors to the $\beta 2$ subunit

A comparison of the hydrogen-bonding donor-acceptor pairs and of the related interaction distances for TMC-95A and the analogue **2a** in the $\beta 2$ subunit (Table 4) reveals that the strong hydrogen bond (2.5 \AA) between the C=O moiety of the N-terminal amide of TMC-95A and the side-chain carboxamide of Gln22 of the protein is replaced by a weaker hydrogen bond (3.6 \AA) between the Tyr C=O of **2a** and the Gln22 carboxamide. All other hydrogen bonds are identical for both ligands. The superimposition of the crystal structures of **2a** and TMC-95A in the $\beta 2$ active site (Figure 4) reveals a slight shift of the biaryl

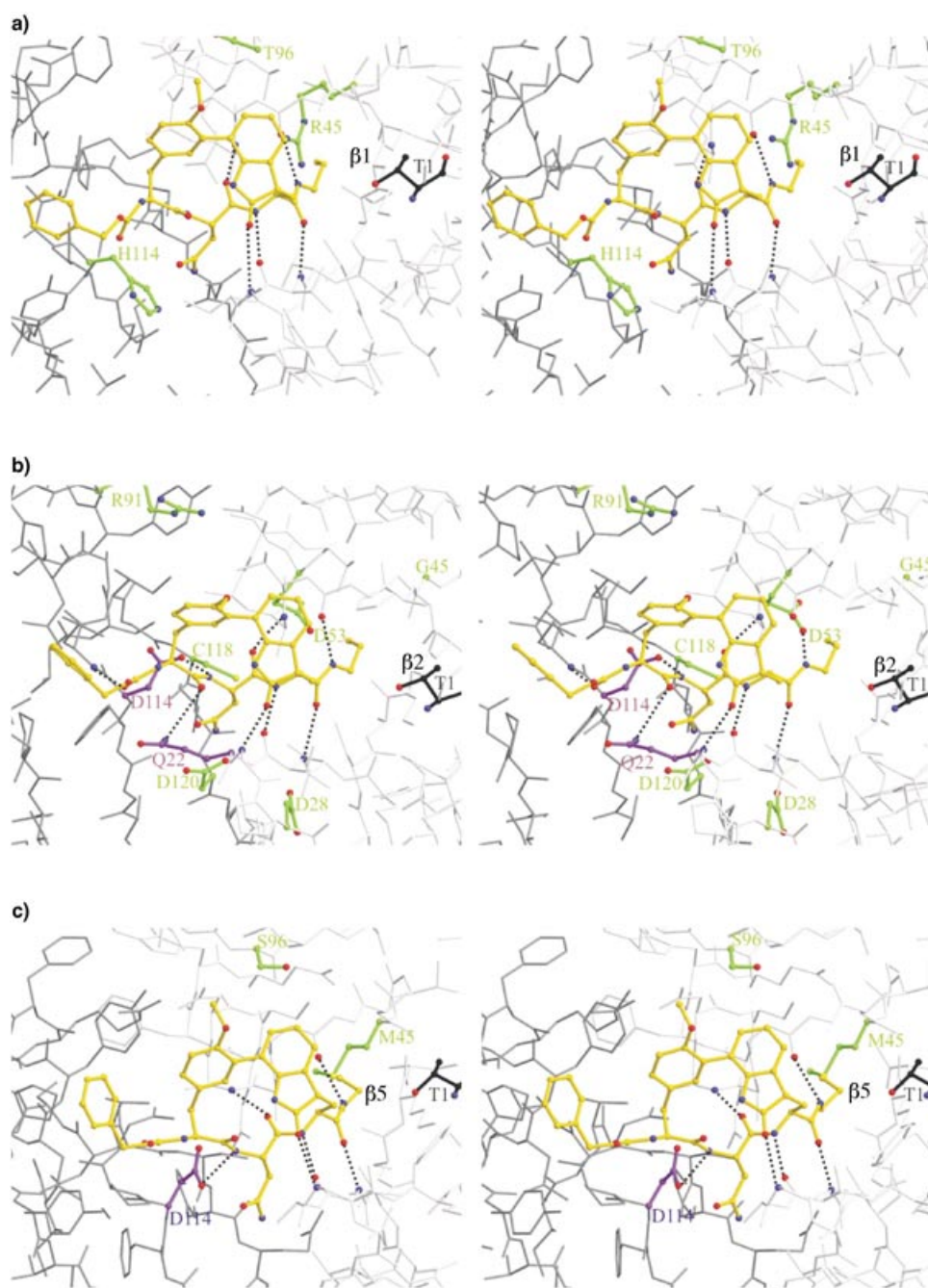


Figure 3. Stereoview of a 30 Å sector of the crystal structures of the a) $\beta 1$, b) $\beta 2$, and c) $\beta 5$ active sites of yeast 20S proteasome in complex with the inhibitor **2a**.

moiety, but an almost identical display of the peptide backbone and of the C-terminal amide—the main components of the hydrogen-bonding network. In both complexes a water molecule is bound to Thr21, Gly23, and Tyr24 of the $\beta 3$ subunit. This water molecule is hydrogen bonded to O42 (Trp γ OH) of TMC-95A but not to **2a** where the two hydroxy groups are missing. Moreover, differences are detectable in the mode of insertion of the (*Z*)-prop-1-enyl moiety of TMC-95A and the *n*-propyl group of **2a** into the S1 binding pocket, whereas the Asn side chain is oriented in an identical manner for both inhibitors (Figure 4). The results suggest that the lower affinity of

2a relative to TMC-95A results from the loss of the water-mediated hydrogen bond and a weaker hydrogen bond involving the N-terminus of the ligand, and more decisively from the entropic penalty that derives from the flexible *n*-propyl chain replacing the conformationally restricted (*Z*)-prop-1-enyl group as the P1 residue.

The overall binding mode of **2b** to the $\beta 2$ subunit is very similar to that of **2a** (Figure 4). The hydrogen bond between the Asn side chain of **2a** and the protein Gln22 is lost in **2b** because of the Asn/Leu replacement (Table 4). Moreover, conversion of the C-terminal amide to a carboxylate group should lead to solvation of the anion and thus to entropic costs which together with those derived from insertion of the long flexible Nle *n*-butyl chain into the S1 pocket can well account for the significantly weaker binding of **2b** compared to **2a**.

Binding of inhibitors to the $\beta 5$ subunits

The crystal structures of yeast CP in complex with TMC-95A and **2a** reveal an identical hydrogen-bonding pattern in the $\beta 5$ subunits (Table 4). The Asn side chain and peptide backbones of both inhibitors are fully superimposable (Figure 4), whereas the biaryl system of **2a** is slightly shifted but still retains the oxindole in hydrogen-bonding distance to Gly23 NH as in TMC-95A. The main differences are observed in the display of the C-terminal carboxamide group and of the *N*-alkyl chains that protrude into the S1 pocket. A bound water molecule was not detected in the interface between the biaryl system and the protein surface, although there would be sufficient space. Correspondingly, the Trp γ OH (O42) residue is not involved in a hydrogen bond to the protein surface as was observed for TMC-95A bound to the $\beta 2$ subunit. If desolvation of the two hydroxy groups of TMC-95A in the bound state indeed occurs, binding of TMC-95A to the $\beta 5$ active site could be substantially favored by the gain of entropy resulting from released water molecules. In fact, reorganization of the water

Table 3. Crystallographic data collection and refinement statistics.		
Parameter	Proteasome/2a	Proteasome/2b
Space group	P2 ₁	P2 ₁
a [Å]	136.0	135.4
b [Å]	300.2	300.8
c [Å]	144.3	143.9
β [°]	113	112.9
Resolution [Å]	15–3.1	15–2.6
Observation (2σ)	576890	1039309
Uniques	198643	325229
Completeness [%]	96.6	95.8
R _{merge} /last resolution shell [%]	11.3/47.1	6.3/43.1
R _{crys} /R _{free} [%]	21.3/25.2	22.3/23.7
Rms bonds [Å]	0.007	0.006
Rms angles [°]	1.27	1.296

S1 pocket without any steric clashes, whereas the *n*-propyl chain is deeply inserted, thus clashing with the side chain of Met45.

A comparison of the structures of lactacystin and the norleucinal tripeptide bound to yeast CP clearly revealed structural rearrangements of Met45 induced by larger-sized P1 residues.^[2b] Such an effect is also observed with the inhibitor **2b**. Although the Met45 side chain is partly displaced (Figure 2b), the steric clash in the S1 pocket acts like a lever on the C-terminal Nle residue and on the biaryl group and pushes the peptide backbone away from the binding position in the active site cleft. In particular, the C-terminal amide is displaced from the active site Thr1γOH and is not correctly positioned for hydrolysis to occur. Therefore, the observed deamidation of **2b** is likely to occur at the β2 trypsin-like active sites. Since the

carboxylate group is withdrawn from the active site, it should not affect the binding affinity as strongly as in the β2 subunit.

In a preceding study, the (*Z*)-prop-1-enylamide of TMC-95A was replaced with the ketomethylene moiety Nleψ[COCH₂]-Gly-Ala-Ala-NH₂ to span the active site and to possibly exploit interactions with the S' subsites of the β5 subunit.^[14] This C-terminal extension was expected to increase the inhibitory potency; however, the opposite effect was observed—a fact that can now be explained rationally by the binding mode of the precursor molecule **2b**.

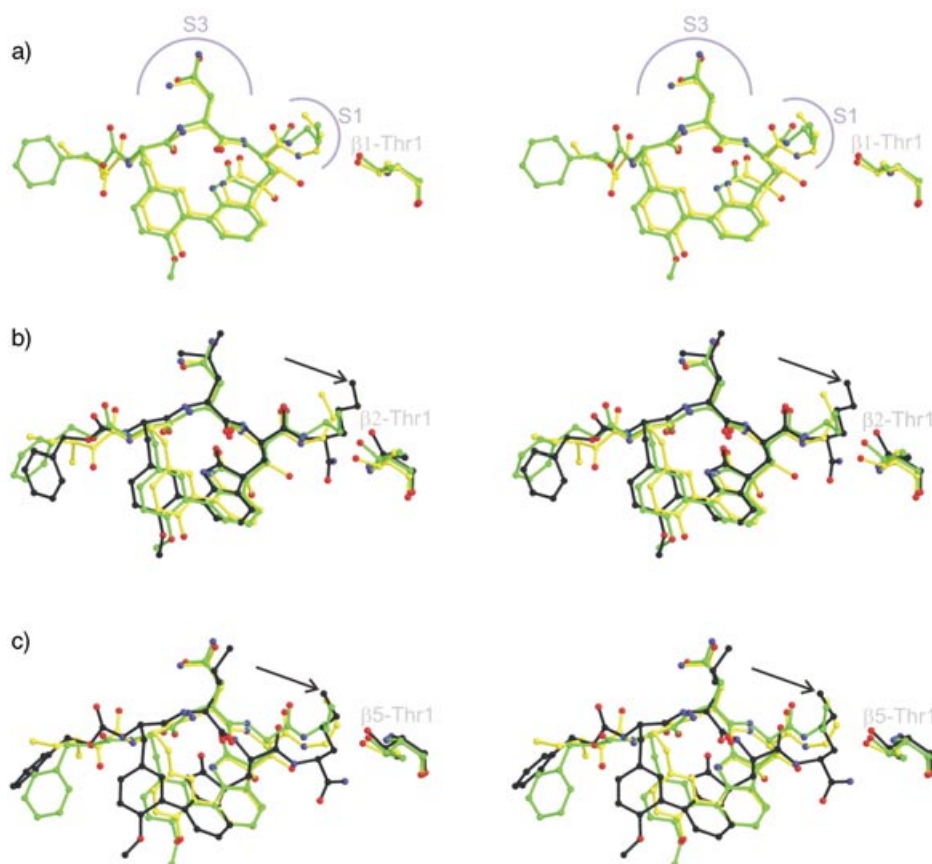
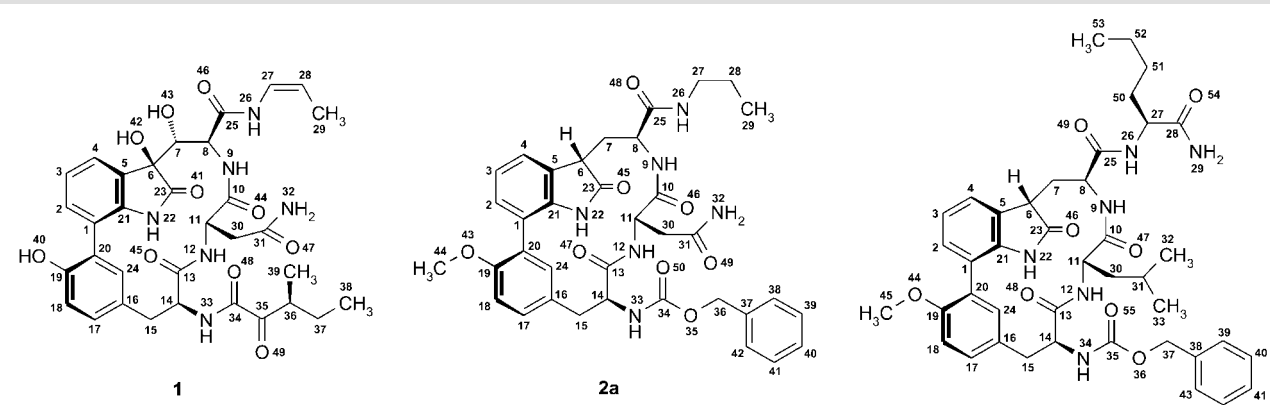


Figure 4. Stereoview of the superimposed structures of TMC-95A (yellow), **2a** (green), and **2b** (black) bound to the active sites of a) β1, b) β2, and c) β5 subunit. In the β2 active site (b), the black arrow indicates that insertion of the P1 residue into the large S1 pocket is not limited, whereas in the S1 pocket of the β5 subunit (c), the residues are inserted to identical depth.

is known to contribute substantially to the binding enthalpy,^[20] and release of one water molecule is accompanied by an entropy gain of up to 28 J mol⁻¹ K⁻¹.^[21] In addition to the lack of this potential entropy gain for **2a**, the more flexible *n*-propyl P1 residue (cf. the (*Z*)-prop-1-enyl moiety in TMC-95A) has to account for the rather weak binding affinity of **2a**. The (*Z*)-prop-1-enyl group of TMC-95A optimally fills the hydrophobic

TMC-95A remains at a distance of 4.3 Å. As a consequence, both the entropic penalty derived from the more flexible *n*-propyl group and the unfavorable interaction with the guanidino group have to account for the significantly lower binding of **2a** compared to TMC-95A. Because of the close proximity to the charged guanidino group observed with the *n*-propyl group, it is not surprising that further elongation of the P1

Table 4. Interacting distances (r) between inhibitors and protein in the $\beta 1$, $\beta 2$, and $\beta 5$ active sites.


Inhibitor	Subunit	r [Å]	Subunit	r [Å]	Subunit	r [Å]
TMC-95 (1)	N26–CO/G47($\beta 1$)	3.0	N26–CO/G47($\beta 2$)	3.1	N26–CO/G47($\beta 5$)	2.9
	O46–N/T21($\beta 1$)	3.0	O46–N/T21($\beta 2$)	2.9	O46–N/T21($\beta 5$)	2.8
	N9–CO/T21($\beta 1$)	2.9	N9–CO/T21($\beta 2$)	2.7	N9–CO/T21($\beta 5$)	2.8
	O41–N/G23($\beta 1$)	3.8	O41–N/G23($\beta 2$)	3.1	O41–N/G23($\beta 5$)	4.0
	O44–N/T49($\beta 1$)	2.8	O44–N/A49($\beta 2$)	3.1	O44–N/A49($\beta 5$)	3.3
				O48–N/L115($\beta 3$)	4.1	
2a	N26–CO/G47($\beta 1$)	3.0	N26–CO/G47($\beta 2$)	3.0	N26–CO/G47($\beta 5$)	2.8
	O48–NH/T21($\beta 1$)	3.0	O48–N/T21($\beta 2$)	2.8	O48–N/T21($\beta 5$)	3.0
	N9–CO/T21($\beta 1$)	2.9	N9–CO/T21($\beta 2$)	2.8	N9–CO/T21($\beta 5$)	2.8
	O45–NH/G23($\beta 1$)	3.8	O45–N/G23($\beta 2$)	3.0	O45–N/G23($\beta 5$)	4.0
	O46–NH/T49($\beta 1$)	3.0	O46–N/A49($\beta 2$)	2.7	O46–N/A49($\beta 5$)	3.3
			O50–N/L115($\beta 3$)	3.9		
			O47–Q22Ne2($\beta 2$)	3.6		
			N12–D114O δ 1/2($\beta 3$)	3.1	N12–D114O δ 1/2($\beta 6$)	3.1
2b	no binding		N26–CO/G47($\beta 2$)	2.8	N26–CO/G47($\beta 5$)	2.5
			N9–CO/T21($\beta 2$)	2.9	N9–CO/T21N($\beta 5$)	4.5
			O49(OK)–N/T21($\beta 2$)	4.1	O49–N/T21($\beta 5$)	4.5
			O46–N/G23($\beta 2$)	3.2	O46–N/G23($\beta 5$)	5.7
			O47–N/A49($\beta 2$)	3.2	O47–N/A49($\beta 5$)	3.3
			N12–D114O δ 1($\beta 3$)	3.0	N12–D114O δ 1($\beta 6$)	3.4
			O55–N/Leu115($\beta 3$)	2.5	O54–N/G47($\beta 5$)	2.7

alkyl chain with the Nle residue in **2b** abolishes binding to this active site.

Discussion

The resolution of the crystallographic analysis obtained for the yeast CP–inhibitor complexes (2.6–3.1 Å) accounts for an error in the protein–ligand bond distances of a few tenths of an ångström.^[22] Although this uncertainty precludes a clear distinction between more or less efficient hydrogen bonds, the measured distances nevertheless provide valuable guidelines.

The differences in affinity of TMC-95A for the three subunits is likely due to the nature of the P1 and P3 residues and their spatial display by the bound rigid core structure. In this context the conformationally restricted (*Z*)-prop-1-enyl chain (P1 residue) of the natural product appears to play a decisive role, since the Asn side chain (P3 residue) is inserted into the S3

pocket in an almost identical manner in all three active sites. The hydrophobic S1 pocket of the $\beta 5$ active site (chymotrypsin-like activity) is occluded by Met45 and thus limited in size, whereas in the S1 pocket of $\beta 1$ the charged Arg45 dominates the electrostatic properties and generates the caspase-like activity. It is well established that efficient occupation of binding pockets by shape- and charge-complementary ligand moieties substantially dictates affinities for the receptor molecule. Since the P1 residues of TMC-95A and **2a** are both hydrophobic, but differ in the degrees of conformational flexibility, the loss of entropy for the *n*-propyl in the bound state of **2a** is apparently not compensated by the enthalpy of binding. The *n*-propyl groups in the S1 subsites of $\beta 5$ and $\beta 1$ are well defined, but different from that of the (*Z*)-prop-1-enyl chain (Figure 4). While the (*Z*)-prop-1-enyl group optimally fills these pockets with its bent conformation, the *n*-propyl chain is deeply inserted in a well-defined extended conformation into the S1 sub-

sites in close proximity to Met45 of the $\beta 5$ active center and to the charged Arg45 guanidino group of $\beta 1$. The steric clashes with Met45 of $\beta 5$ and the unfavorable proximity to a charged residue in $\beta 1$ are even worse in the case of compound **2b** whose *n*-butyl side chain was found to displace the peptide backbone from the ideal alignment with the active site cleft of $\beta 5$ and thus to further weaken the binding affinity. In the case of the $\beta 1$ active site, the analogue **2b** loses its inhibitory activity completely.

Conclusion

The main message derived from this study is that the restricted conformational freedom of the cyclic tripeptide dictates the mode of insertion of residues into pockets of the active site cleft and, correspondingly, the optimal occupancy of critical binding subsites. In fact, the rigid display of the backbone severely limits the choice of groups acting as P1 residues without steric clashes. Thus, the use of other possibly less bulky and less rigid endocyclic clamps for conformational restriction of the peptide backbone could allow better orientation of groups interacting with the various subsites. Promising results along these lines have been obtained by incorporating an isodityrosine-type biaryl ether,^[23] which is also known to restrict the peptide backbone in a β -type extended conformation,^[24] into the TMC-95A tripeptide.

Experimental Section

Materials and methods: Reagents and solvents were of the highest quality commercially available and were used without further purification. All amino acids are of L configuration. TLC was carried out on silica gel 60F₂₅₄ precoated glass plates (Merck, Darmstadt, Germany). Analytical HPLC was performed on I) X-Terra-MS C8 5 μ m column (150 \times 3.9 mm) from Waters, II) Luna C₁₈ 5 μ m column (150 \times 4.6 mm) from Phenomenex (Aschaffenburg, Germany), and III) Chromolith C₁₈ 5 μ m column (100 \times 4.6 mm) from Merck (Darmstadt, Germany) using linear gradients from 5% MeCN in 2% aq. H₃PO₄ to 90% MeCN in 2% aq. H₃PO₄ in 15 min (I, II) or 7 min (III) at flow rates of 1 (I), 1.5 (II), and 3 mL min⁻¹ (III). For preparative reverse-phase (RP) HPLC, a Nucleosil C₈ SP250/10 column (Macherey & Nagel, Düren, Germany) and gradients from 0.1% aq. TFA to MeCN containing 0.1% TFA (flow rate 3 mL min⁻¹) were used. ESI mass spectra were recorded on a PE Sciex API165 instrument. Routine ¹H NMR spectra of intermediate products were recorded at 27 °C on a Bruker AMX 400 spectrometer and are consistent with the assigned structures.

Synthesis of TMC-95A analogue 2a

Boc-Trp(7-Br)-NHPr (3): Diisopropylethylamine (DIEA; 280 μ L, 1.63 mmol), 1-hydroxybenzotriazole hydrate (HOBT·H₂O; 250 mg, 1.63 mmol), and *N*'-ethyl-*N*'-(3-dimethyl-aminopropyl)carbodiimide hydrochloride (EDCI; 310 mg, 1.63 mmol) were added to a solution of Boc-Trp(7-Br)-OH (570 mg, 1.49 mmol) in *N,N*-dimethylformamide (DMF; 30 mL). After stirring for 10 min at room temperature (RT), *n*-propylamine (150 μ L, 1.78 mmol) was added, and the mixture was kept overnight at RT. The reaction mixture was then concentrated, diluted with EtOAc, and washed with 5% aq. NaHCO₃, 5% aq. KHSO₄, and brine. After drying (Na₂SO₄), the organic layer was evaporated to dryness to afford the title compound (574 mg,

91% yield). TLC (CHCl₃/MeOH, 9:1): *R*_f = 0.55; HPLC (I): *t*_R = 11.00 min; ESI-MS: *m/z* calcd for C₁₉H₂₆BrN₃O₃: 423.34, 425.34; found: 424.2 [*M*(⁷⁹Br)+H]⁺, 426.2 [*M*(⁸¹Br)+H]⁺.

Boc-{7-[3'-(Z-Tyr(Me)-OH)]}Trp-NHPr (4): A solution of **3** (270 mg, 0.64 mmol), Z-Tyr(3-boronic pinacol ester, 4-Me)-OMe^[14] (450 mg, 0.95 mmol), and K₂CO₃ (260 mg, 1.91 mmol) in DMF/water (7:1, 30 mL) was degassed and then saturated with argon. [Pd(dppf)Cl₂]-CH₂Cl₂ (dppf = 1,1'-bis(diphenylphosphino)ferrocene; 20 mg, 0.02 mmol) was added, and the mixture was kept for 10 h at 90 °C. Upon cooling to RT, the mixture was acidified with 5% aq. KHSO₄ (30 mL) and extracted with EtOAc (3 \times 30 mL). The combined organic extracts were washed with water and brine, dried (Na₂SO₄), and evaporated to dryness. The residue was purified by chromatography on silica gel (CHCl₃/MeOH, 9:1) to afford the title compound (351 mg, 81% yield) as a yellowish powder. TLC (CHCl₃/MeOH, 9:1): *R*_f = 0.52; HPLC (II): *t*_R = 11.28 min; ESI-MS: *m/z* calcd for C₃₇H₄₄N₄O₈: 672.79; found: 673.7 [*M*+H]⁺.

Boc-{7-[3'-(Z-Tyr(Me)-Asn-OrBu)]}Trp-NHPr (5): H-Asn-OrBu-HCl (80 mg, 0.34 mmol) was added to a solution of **4** (210 mg, 0.31 mmol), DIEA (110 μ L, 0.67 mmol), HOBT·H₂O (50 mg, 0.34 mmol), and EDCI (70 mg, 0.34 mmol) in DMF (30 mL). After stirring overnight at RT, the mixture was evaporated to dryness. The residue was dissolved in EtOAc (30 mL) and washed with 5% aq. NaHCO₃, 5% aq. KHSO₄, and brine. The organic layer was dried (Na₂SO₄) and evaporated to dryness to afford the title compound (240 mg, 92% yield) as a white solid. TLC (CHCl₃/MeOH, 9:1): *R*_f = 0.43; HPLC (II): *t*_R = 11.46 min; ESI-MS: *m/z* calcd for C₄₅H₅₇N₅O₁₁: 843.97; found: 844.9 [*M*+H]⁺.

H- β -{7-[3'-(Z-Tyr(Me)-Asn-OH)]}oxindolylalanine-NHPr-HCl (6): Compound **5** (180 mg, 0.21 mmol) was dissolved in glacial AcOH/conc. HCl (4:1, 20 mL) and then treated with dimethyl sulfoxide (DMSO; 360 μ L, 0.42 mmol). After 2 h at RT, the solution was co-evaporated to dryness from toluene (twice), and the crude product was purified by preparative HPLC. The title compound (80 mg, 49% yield) was isolated as the lyophilizate from *t*BuOH/water (4:1). HPLC (II): *t*_R = 6.42 min; ESI-MS: *m/z* calcd for C₃₆H₄₁N₅O₁₀: 703.76; found: 704.7 [*M*+H]⁺.

TMC-95A analogue 2a: A solution of **6** (80 mg, 0.11 mmol) and DIEA (20 μ L, 0.11 mmol) in DMF (50 mL) was added over 30 min to a stirred (degassed and then) argon-saturated solution of (benzotriazol-1-yl-oxy)-tris(pyrrrolidino)phosphonium hexafluorophosphate (PyBOP; 230 mg, 0.44 mmol), DIEA (80 μ L, 0.44 mmol), and HOBT·H₂O (70 mg, 0.44 mmol) in DMF (250 mL). After 24 h at RT, the reaction mixture was evaporated, and the residue was purified by preparative HPLC. The title compound (30 mg, 33% yield) was isolated as the lyophilizate from *t*BuOH/water (4:1). TLC (CHCl₃/MeOH, 8:2): *R*_f = 0.34; HPLC (II): *t*_R = 9.90 min; ESI-MS: *m/z* calcd for C₃₆H₃₉N₅O₉: 685.75; found: 686.7 [*M*+H]⁺; ¹H NMR (500 MHz, [D₆]DMSO): δ = 8.86 (d, *J* = 7.9 Hz, 1H; Asn^{NH}), 8.21 (s, 1H; Trp^{indole}), 7.90 (d, *J* = 9.3 Hz, 1H; Trp^{NH}), 7.52 (t, 1H; propylamide^{NH}), 7.43, 7.08 (2s, 2H; Asn^{NH2}), 7.38 (s, 5H; Z^{anom}), 7.19 (d, *J* = 7.7 Hz, 1H; Trp^{C8}), 7.19 (s, 1H; Tyr^{C2}), 7.13 (d, *J* = 7.7 Hz, 1H; Trp^{C6}), 6.98 (t, *J* = 7.7 Hz, 1H; Trp^{C7}), 6.95 (d, *J* = 8.6 Hz, 1H; Tyr^{C6}), 6.92 (d, *J* = 8.6 Hz, 1H; Tyr^{C5}), 5.78 (m, ³*J*_{N α} = 7.7 Hz, 1H; Tyr^{NH}), 5.10, 5.03 (2d, *J* = 12.6 Hz, 2H; Z^{CH2}), 4.63 (m, 1H; Asn ^{α}), 4.53 (m, 1H; Tyr ^{α}), 3.85 (m, 1H; Trp ^{α}), 3.70 (s, 3H; Tyr^{O-CH3}), 3.60 (t, 1H; Trp ^{γ}), 3.07 (dd, *J* _{$\beta\beta$} = 12.8 Hz, 1H; Tyr^{OCH3}), 3.01, 2.96 (m, 2H, propylamide^{CH3}), 2.90 (dd, *J* _{$\alpha\beta$} = 4 Hz, 1H; Tyr ^{β}), 2.62, 2.51 (dd, 2H; Asn ^{β}), 2.58 (t, 1H; Trp ^{β}), 2.35 (dd, 1H; Trp ^{β}), 1.35 (m, 2H; propylamide^{CH2}), 0.78 (t, 3H; propylamide^{CH3}) ppm.

Synthesis of TMC-95A analogue 2b

Boc-Trp(7-Br)-Nle-NH₂ (7): Dicyclohexylcarbodiimide (DCC) (86.7 mg, 0.42 mmol) and HOBt·H₂O (64.3 mg, 0.42 mmol) were added to a solution of Boc-Trp(7-Br)-OH (160 mg, 0.42 mmol) in CH₂Cl₂ (5 mL), and the mixture was stirred for 30 min at RT. The urea was filtered off, and H-Nle-NH₂-trifluoroacetate (103 mg, 0.42 mmol) in CH₂Cl₂ (3 mL) and DIEA (72 μL, 0.42 mmol) were added to the filtrate. The mixture was stirred overnight and then evaporated to dryness. The title compound (178 mg, 90% yield) was isolated as described for **3**. TLC (CHCl₃/MeOH, 6:1): *R_f* = 0.42; HPLC (III): *t_R* = 3.63 min; ESI-MS: *m/z* calcd for C₂₂H₃₁BrN₄O₄: 494.42, 496.42; found: 495.2 [M(⁷⁹Br)+H]⁺, 497.2 [M(⁸¹Br)+H]⁺

Boc-[7-[3'-(Z-Tyr(Me)-OH)]Trp-Nle-NH₂ (8): [Pd(dppf)Cl₂]-CH₂Cl₂ (20 mg, 0.02 mmol) was added to a stirred (degassed and then) argon-saturated solution of **7** (300 mg, 0.61 mmol), Z-Tyr(3-boronic pinacol ester,4-Me)-OMe^[14] (570 mg, 1.21 mmol), and K₂CO₃ (250 mg, 1.83 mmol) in DMF/water (7:1, 50 mL), and the mixture was kept for 10 h at 90 °C. Upon cooling to RT, the mixture was acidified with 5% aq. KHSO₄ (30 mL) and extracted with EtOAc (3 × 30 mL). The combined extracts were washed with 5% aq. KHSO₄ and brine, dried (Na₂SO₄), and evaporated to dryness. The residue was purified by chromatography on silica gel with a linear gradient from CH₂Cl₂/MeOH (9:1) to CH₂Cl₂/MeOH (4:1) to afford the title compound (295.5 mg, 65% yield) as a yellowish solid. TLC (CHCl₃/MeOH, 9:1): *R_f* = 0.32; HPLC (III): *t_R* = 3.93 min; ESI-MS: *m/z* calcd for C₄₀H₄₉N₅O₉: 743.86; found: 744.8 [M+H]⁺.

Boc-[7-[3'-(Z-Tyr(Me)-Leu-OrtBu)]Trp-Nle-NH₂ (9): H-Leu-OrtBu-HCl (80 mg, 0.35 mmol) was added to a solution of **8** (200 mg, 0.27 mmol), DIEA (110 μL, 0.62 mmol), HOBt·H₂O (50 mg, 0.35 mmol), and EDCl (70 mg, 0.35 mmol) in DMF (25 mL). The reaction mixture was stirred overnight at RT and worked up as described for **5** to afford the title compound (207 mg, 85% yield). TLC (CHCl₃/MeOH, 9:1): *R_f* = 0.34; HPLC (III): *t_R* = 5.05 min; ESI-MS: *m/z* calcd for C₅₀H₆₇N₅O₁₁: 913.12; found: 914.2 [M+H]⁺.

H-β-[7-[3'-(Z-Tyr(Me)-Leu-OH)]Joxindolylalanyl-Nle-NH₂-HCl (10): DMSO (274 μL, 3.2 mmol) was added to compound **9** (140 mg, 0.16 mmol) in glacial AcOH/conc. HCl (4:1, 25 mL), and the mixture was kept at RT for 2 h. The solution was co-evaporated to dryness from toluene (twice), and the residue was purified by preparative HPLC. The title compound (39 mg, 54% yield) was isolated as the lyophilizate from tBuOH/water (4:1). HPLC (III): *t_R* = 3.08 min; ESI-MS: *m/z* calcd for C₄₁H₅₂N₅O₁₀: 773.89; found: 774.8 [M+H]⁺.

TMC-95A analogue 2b: A solution of **10** (70 mg, 0.08 mmol) and DIEA (14 μL, 0.08 mmol) in DMF (35 mL) was added over 30 min to a stirred (degassed and then) argon-saturated solution of PyBOP (160 mg, 0.32 mmol), DIEA (110 μL, 0.64 mmol), and HOBt·H₂O (50 mg, 0.32 mmol) in DMF (250 mL). After 36 h at RT, the reaction mixture was evaporated to dryness, and the residue was purified by preparative HPLC. The title compound (23 mg, 38% yield) was isolated as the lyophilizate from tBuOH/water (4:1). TLC (CHCl₃/MeOH, 8:2): *R_f* = 0.39; HPLC (III): *t_R* = 3.74 min; ESI-MS: *m/z* calcd for C₃₉H₄₄N₆O₁₀: 756.82; found: 757.7 [M+H]⁺; ¹H NMR (500 MHz, [D₆]DMSO): δ = 8.75 (d, *J* = 7.3, 1 H; Leu^{NH}), 8.20 (d, *J* = 9.2 Hz, 1 H; Trp^{NH}), 8.17 (s, 1 H; Trp^{indole}), 7.40 (s, 5 H; Z^{arom}), 7.32, 7.30 (m, 2 H; C-term^{NH₂}), 7.20, 7.12 (d, *J* = 7.3 Hz, 2 H; Trp^{C₆,C₈}), 7.12 (s, 1 H; Tyr^{C₂}), 7.04 (m, 1 H; Nle^{NH}), 6.97 (m, 1 H; Trp^{C₇}), 6.95 (m, 2 H; Tyr^{C₃,C₄}), 5.95 (d, 1 H; Tyr^{H_N}), 5.15, 5.00 (2d, *J* = 12.6 Hz, 2 H; Z^{CH₂}), 4.5 (m, 1 H; Tyr^α), 4.24 (m, 1 H; Leu^α), 4.17 (m, 1 H; Nle^α), 3.86 (m, 1 H; Trp^α), 3.70 (s, 3 H; Tyr^{OCH₃}), 3.61 (t, 1 H; Trp^γ), 3.10 (m, 1 H; Tyr^β), 2.94 (m, 1 H; Tyr^β), 2.50 (m, 1 H; Trp^β), 2.42 (m, 1 H; Trp^β), 1.73 (m, 1 H; Leu^γ), 1.61 (m, 1 H; Nle^β), 1.59 (m, 1 H; Leu^β), 1.53 (m, 1 H; Leu^β), 1.45 (m, 1 H;

Nle^β), 1.24 (m, 2 H; Nle^β), 1.19 (m, 2 H; Nle^γ), 0.88 (m, 6 H; Leu^δ), 0.87 (m, 3 H; Nle^δ) ppm.

Enzyme kinetics: Inhibition of the trypsin-like, chymotrypsin-like, and PGPH activities of yeast proteasome was evaluated by following the protocols described elsewhere^[14] but using the following substrates: Z-Ala-Arg-Arg-AMC, Suc-Leu-Leu-Val-Tyr-AMC, and Z-Leu-Leu-Glu-βNa, respectively. For monitoring hydrolysis of **2b**, the inhibitor was incubated at 37 °C at a concentration of 104 μM in 20 mM HEPES buffer (pH 7.5) containing 0.5 mM EDTA, 0.025% SDS, and 5% DMSO in the presence of 52 μM Suc-Leu-Leu-Val-Tyr-AMC as substrate and 10 nM yeast proteasome. Hydrolysis of the inhibitor to the related carboxy derivative was monitored by HPLC of aliquots taken at suitable time intervals. Under these conditions a *t_{1/2}* value of 27 min was derived.

NMR spectroscopy: NMR experiments for conformational analysis were carried out at 22 °C on a Bruker DRX500 spectrometer in [D₆]DMSO. Resonance assignments were performed according to Wüthrich's method.^[25] The 2D TOCSY spectra were recorded with spin-lock periods of 70–75 ms using the MLEV-17 sequence for isotropic mixing.^[26] Experimental interproton distance constraints (**2a**: 45, **2b**: 36) were extracted from 2D-ROESY experiments^[27] with a mixing time of 200 ms. Three ³*J*_{HN-Hα} coupling constants were derived for each TMC-95A analogue from 2D double quantum filtered correlation spectroscopy (2D-DQF-COSY)^[28] and simple 1D ¹H NMR spectra.

Structure calculations: Distance geometry and MD simulated annealing calculations were performed with the INSIGHT II (version 98.0) software package from MSI on Silicon Graphics O2 R5000 computers. One hundred structures were generated from the distance-bound matrices. Triangle-bound smoothing was used. The NOE intensities were converted into interproton distance constraints by using the following classification: very strong (vs) 1.7–2.3 Å, strong (s) 2.2–2.8 Å, medium (m) 2.6–3.4 Å, weak (w) 3.0–4.0 Å, and very weak (vw) 3.2–4.8 Å; and the distances of pseudoatoms were corrected as described by Wüthrich.^[25] The ³*J*_{HN-Hα} coupling constants were converted into constraints for the backbone ϕ dihedral angles by using the Karplus relationship. Multiple discrete ranges were used for the ϕ torsion angle restraints when multiple nonoverlapping solutions existed for the Karplus equation taking into account experimental error and 5° uncertainty from the Karplus parameters. The structures were generated in four dimensions. These were then reduced to three dimensions with the EMBED algorithm^[29] and optimized with a simulated annealing step^[30] according to the standard protocol of the distance geometry II package from INSIGHT II. All one hundred structures were refined with a short MD simulated annealing protocol: after an initial minimization, 5 ps at 300 K were simulated followed by exponential cooling to ≈0 K during 10 ps. A time step of 1 fs was used with the consistent valence force field (CVFF) while simulating the solvent DMSO with a dielectric constant of 46.7. The experimental constraints were applied at every stage of the calculation with 50 kcal mol⁻¹ Å⁻² for distance constraints and 50.0 kcal mol⁻¹ rad⁻² for coupling constants. Violations of experimental NOE constraints were all below 0.2 Å for the ten lowest-energy structures.

Protein purification and X-ray analysis: The yeast 20S proteasome was purified by using a β2-TEV-ProA-tagged mutant. The strain was prepared by homologous recombination according to known procedures.^[31] The plasmid containing the TEV-ProA (tobacco edge virus protease/protein A construct) and Geneticin modules was a gift from Dr. Knop, Heidelberg. Standard techniques were used for DNA manipulations.^[32] Standard PCR reactions (hot start)

using Taq polymerase and Taq buffer provided by various suppliers were used for amplification of the modules using designed primers. The annealing temperature was 54 °C; the elongation time was 1 min per 1 kb of DNA. Fractions (2–5 μL) of the PCR reactions were analyzed by agarose gel electrophoresis. The residual reaction was precipitated with ethanol, and the DNA was resuspended in water (15 μL). From this, 3–5 μL was used to transform competent yeast cells. The transformation protocol was based on the LiOAc method.^[33] Yeast cells of this mutant were grown for at least 6–8 h (or overnight) to an optical density of 0.5–1.5 (600 nm) at 30 °C in YPAD medium (1% yeast extract, 2% peptone, and 2% glucose supplemented with 100 mg mL⁻¹ adenine).

Cells were harvested, resuspended in a twofold volume of buffer 1 (50 mM Tris-HCl, pH 8, 1 mM EDTA), and lysed by French press. Lysate was clarified at 15000g for 25 min, incubated with IgG resin (ICN, Eschwege, Germany) for 1 h at 4 °C, and the resin washed with 50 bed volumes of buffer 2 (50 mM Tris-HCl, pH 7.5, 1 mM EDTA, 500 mM NaCl). At this stage, the proteasome is essentially pure electrophoretically and was eluted by using TEV protease. The yeast CP was generated by washing the IgG resin with 3 volumes of TEV elution buffer (TEB: 50 mM Tris-HCl, pH 7.5, 1 mM EDTA, 1 mM DTT), then incubating with 1.5 volumes of TEB buffer containing 150 U of 6His-TEV protease at 30 °C for 1 h. The enzymes were eluted with TEB buffer, and the TEV protease was removed by incubation with nickel-NTA resin (Qiagen, Hilden, Germany) at 4 °C for 15 min. The CP was further purified by using a Superose 6 (Pharmacia, Freiburg, Germany) size-exclusion chromatography. Crystals of the CP were grown in hanging drops at 20 °C as described elsewhere.^[2b] The crystals were soaked at final inhibitor concentrations of at least 5 mM for 12 h in a cryoprotecting buffer and frozen in a stream of liquid nitrogen gas (Oxford Cryo Systems, Oxford, UK). Data were collected by using synchrotron radiation with $\lambda = 1.1 \text{ \AA}$ on the BW6-beamline at the Deutsches-Elektronen-Synchrotron, Hamburg, Germany. The anisotropy of diffraction was corrected by an overall anisotropic temperature factor by comparing observed and calculated structure amplitudes using the program CNS.^[34] The electron density was averaged ten times over the twofold noncrystallographic symmetry axis, and model building was carried out by using MAIN.^[35] The data collection and crystallographic refinement statistics for complexes of yeast proteasome with the TMC-95A analogues yielded $R_{\text{cryst}}/R_{\text{free}} = 21.3/25.2\%$ (15–3.1 \AA resolution, R_{merge} overall 11.3) for CP:2a and $R_{\text{cryst}}/R_{\text{free}} = 22.3/23.7\%$ (15–2.6 \AA resolution, R_{merge} overall 6.3) for CP:2b (for crystallographic data collection and refinement statistics see Table 3).

The X-ray structures of the yeast proteasome–TMC-95A complexes were refined by iterative model building by using the software package CNS and MAIN to $R_{\text{cryst}} = 21.9\%$ and $R_{\text{free}} = 25.4\%$ and a final resolution of 3.1 \AA compared to $R_{\text{cryst}} = 27.1\%$ and $R_{\text{free}} = 33.6\%$ and the resolution of 3.0 \AA reported previously.^[6a]

Acknowledgements

The help of G. Bourenkow and H. Bartunik (Max-Planck-Arbeitsgruppe, Hamburg) with data collection is gratefully acknowledged. We thank Dr. M. Knop for technical advice in preparing the modified yeast strain and for support in the design of the plasmid constructs. The study was supported by the SFB 469 of the Ludwig-Maximilians Universität Munich (grants A1, A2, and A6).

Keywords: 20S proteasome • binding affinities • conformation analysis • enzyme inhibitors • X-ray diffraction

- [1] a) K. L. Rock, A. L. Goldberg, *Annu. Rev. Immunol.* **1999**, *17*, 739–779; b) A. F. Kisselev, A. L. Goldberg, *Chem. Biol.* **2001**, *8*, 739–758; c) J. Adams, *Trends Mol. Med.* **2002**, *8*, S49–S54; d) A. Hershko, A. Ciechanover, *Annu. Rev. Biochem.* **1998**, *67*, 425–479.
- [2] a) J. Löwe, D. Stock, B. Jap, P. Zwickl, W. Baumeister, R. Huber, *Science* **1995**, *268*, 533–539; b) M. Groll, L. Ditzel, J. Löwe, D. Stock, M. Bochtler, H. D. Bartunik, R. Huber, *Nature* **1997**, *386*, 463–471.
- [3] M. Groll, M. Bajorek, A. Kohler, L. Moroder, D. M. Rubin, R. Huber, M. H. Glickman, D. Finley, *Nature Struct. Biol.* **2000**, *7*, 1062–1067.
- [4] a) M. Groll, H. Brandstetter, H. Bartunik, G. Bourenkow, R. Huber, *J. Mol. Biol.* **2003**, *327*, 75–83; b) M. Groll, T. Clausen, *Curr. Opin. Struct. Biol.* **2003**, *13*, 665–673.
- [5] a) W. Heinemeyer, M. Fischer, T. Krimmer, U. Stachon, D. H. Wolf, *J. Biol. Chem.* **1997**, *272*, 25200–25209; b) A. K. Nussbaum, T. P. Dick, W. Keilholz, M. Schirle, S. Stefanovic, K. Dietz, W. Heinemeyer, M. Groll, D. H. Wolf, R. Huber, H. G. Rammensee, H. Schild, *Proc. Natl. Acad. Sci. USA* **1998**, *95*, 12504–12509; c) M. Groll, W. Heinemeyer, S. Jäger, T. Ullrich, M. Bochtler, D. H. Wolf, R. Huber, *Proc. Natl. Acad. Sci. USA* **1999**, *96*, 10976–10983; d) M. Orlowski, S. Wilk, *Arch. Biochem. Biophys.* **2000**, *383*, 1–16.
- [6] a) M. Groll, Y. Koguchi, R. Huber, J. Kohno, *J. Mol. Biol.* **2001**, *311*, 543–548; b) M. Groll, K. B. Kim, N. Kairies, R. Huber, C. M. Crews, *J. Am. Chem. Soc.* **2000**, *122*, 1237–1238; c) M. Groll, T. Nazif, R. Huber, M. Bogyo, *Chem. Biol.* **2002**, *9*, 655–662.
- [7] a) J. Myung, K. B. Kim, C. M. Crews, *Med. Res. Rev.* **2001**, *21*, 245–273; b) A. L. Goldberg, K. Rock, *Nat. Med.* **2002**, *8*, 338–340.
- [8] a) C. Garcia-Echeverria, P. Imbach, D. France, P. Fürst, M. Lang, M. Noorani, D. Scholz, J. Zimmerman, P. Furet, *Bioorg. Med. Chem. Lett.* **2001**, *11*, 1317–1319; b) P. Furet, P. Imbach, P. Fürst, M. Lang, M. Noorani, J. Zimmerman, C. Garcia-Echeverria, *Bioorg. Med. Chem. Lett.* **2002**, *12*, 1331–1334.
- [9] a) Y. Koguchi, J. Kohno, M. Nishio, K. Takahashi, T. Okuda, T. Ohnuki, S. Komatsubara, *J. Antibiot.* **2000**, *53*, 105–109; b) J. Kohno, Y. Koguchi, M. Nishio, K. Nakao, M. Kuroda, R. Shimizu, T. Ohnuki, S. Komatsubara, *J. Org. Chem.* **2000**, *65*, 990–995.
- [10] M. Kaiser, M. Groll, C. Renner, R. Huber, L. Moroder, *Angew. Chem.* **2002**, *114*, 817–820; *Angew. Chem. Int. Ed.* **2002**, *41*, 780–783.
- [11] K. L. Rock, C. Gramm, L. Rothstein, K. Clark, R. Stein, L. Dick, D. Hwang, A. L. Goldberg, *Cell* **1994**, *78*, 761–771.
- [12] M. Bogyo, S. Shin, J. S. McMaster, H. L. Ploegh, *Chem. Biol.* **1998**, *5*, 307–320.
- [13] A.-C. Carbonnelle, E. G. Zamora, R. Beugelmans, G. Roussi, *Tetrahedron Lett.* **1998**, *39*, 4467–4470.
- [14] M. Kaiser, C. Siciliano, I. Assfalg-Machleidt, M. Groll, A. G. Milbradt, L. Moroder, *Org. Lett.* **2003**, *5*, 3435–3437.
- [15] M. Lee, R. S. Phillips, *Bioorg. Med. Chem. Lett.* **1992**, *2*, 1563–1564.
- [16] G. Loidl, H.-J. Musiol, N. Budisa, R. Huber, S. Poirrot, D. Fourmy, L. Moroder, *J. Pept. Sci.* **2000**, *6*, 139–144.
- [17] a) S. Lin, S. J. Danishefsky, *Angew. Chem.* **2001**, *113*, 2021–2024; *Angew. Chem. Int. Ed.* **2001**, *40*, 1967–1970; b) S. Lin, S. J. Danishefsky, *Angew. Chem.* **2002**, *114*, 530–533; *Angew. Chem. Int. Ed.* **2002**, *41*, 512–515; c) B. K. Albrecht, R. M. Williams, *Org. Lett.* **2003**, *5*, 197–200d) M. Inoue, H. Sakazaki, H. Furuyama, M. Hiram, *Angew. Chem.* **2003**, *115*, 2758–2761; *Angew. Chem. Int. Ed.* **2003**, *42*, 2654–2657.
- [18] Z.-Q. Yang, B. H. B. Kwok, S. Lin, M. A. Koldobskiy, C. M. Crews, S. J. Danishefsky, *ChemBioChem* **2003**, *4*, 508–513.
- [19] M. Unno, T. Mizushima, Y. Morimoto, Y. Tomisugi, K. Tanaka, N. Yasuoka, T. Tsukihara, *Structure* **2002**, *10*, 609–618.
- [20] M. C. Chervenak, E. J. Toone, *J. Am. Chem. Soc.* **1994**, *116*, 10533–10539.
- [21] J. D. Dunitz, *Science* **1994**, *264*, 670.
- [22] a) P. Dauber-Osguthorpe, V. A. Roberts, D. J. Osguthorpe, J. Wolff, M. Genest, A. T. Hagler, *Proteins* **1988**, *4*, 31–47; b) A. Wlodawer, J. Nachman, G. L. Gilliland, W. Gallagher, C. J. Woodward, *J. Mol. Biol.* **1987**, *198*, 469–480.

- [23] M. Kaiser, A. G. Milbradt, C. Siciliano, I. Assfalg-Machleidt, W. Machleidt, M. Groll, C. Renner, L. Moroder, *Chem. Biodiv.* **2004**, *1*, 161–173.
- [24] a) J. W. Janetka, P. Raman, K. Satyshur, G. R. Flentke, D. H. Rich, *J. Am. Chem. Soc.* **1997**, *119*, 441–442; b) J. W. Janetka, K. Satyshur, D. H. Rich, *Acta Crystallogr. Sect. C*, **1996**, *52*, 3112–3114; c) G. Müller, H. Giera, *J. Comp.-Aided Mol. Design* **1998**, *12*, 1–6.
- [25] K. Wüthrich, *NMR of Proteins and Nucleic Acids*, Wiley, New York, **1986**.
- [26] A. Bax, D. G. Davis, *J. Magn. Res.* **1985**, *65*, 355–360.
- [27] A. Bax, D. G. Davis, *J. Magn. Res.* **1985**, *63*, 207–213.
- [28] M. Rance, O. W. Sorensen, G. Bodenhausen, G. Wagner, R. R. Ernst, K. Wüthrich, *Biochem. Biophys. Res. Commun.* **1983**, *117*, 479–485.
- [29] G. M. Crippen, T. F. Havel, *Distance Geometry and Molecular Conformation*, Wiley, New York, **1988**.
- [30] M. Nilges, G. M. Clore, A. M. Gronenborn, *FEBS Lett.* **1988**, *239*, 129–136.
- [31] M. Knop, K. Siegers, G. Pereira, W. Zachariae, B. Winsor, K. Nasmyth, E. Schiebel, *Yeast* **1999**, *15*, 963–972.
- [32] J. Sambrook, E. Fritsch, T. Maniatis, *Molecular Cloning: A Laboratory Manual*, Cold Spring Harbor Laboratory Press, New York, **1989**.
- [33] R. H. Schiestl, R. Gietz, *Curr Genet.* **1989**, *16*, 339–346.
- [34] A. T. Brünger, P. D. Adams, G. M. Clore, W. L. Delano, P. Gros, R. W. Grosse-Kunstleve, J.-S. Jiang, J. Kuszewski, N. Nilges, N. S. Pannu, R. J. Read, L. M. Rice, T. Simonson, G. L. Warren, *Acta Crystallogr. D Biol. Crystallogr.* **1998**, *54*, 905–921.
- [35] D. Turk, *Ph.D. Thesis*, Technical University of Munich, **1992**.

Received: April 6, 2004